Received 27 November 2021; accepted 16 December 2021. Date of publication 22 December 2021; date of current version 4 February 2022.

Digital Object Identifier 10.1109/OJCOMS.2021.3137652

MIMO Per-Tone Equalizer Design for Long Reach xDSL

MOHIT SHARMA [1], JEROEN VERDYCK [2] (Student Member, IEEE), YANNICK LEFEVRE [3], PASCHALIS TSIAFLAKIS [3], AND MARC MOONEN [1] (Fellow, IEEE)

[1]Department of Electrical Engineering (ESAT), STADIUS Center for Dynamical Systems, Signal Processing and Data Analytics, KU Leuven, 3001 Leuven, Belgium

[2]GN Hearing, R&D Global Research Group, 5612 AB Eindhoven, The Netherlands

[3]Fixed Networks Research Antwerp Team, Nokia Bell Labs, 2018 Antwerp, Belgium

CORRESPONDING AUTHOR: M. SHARMA (e-mail: mohitsharma.nith@gmail.com)

This work was supported in part by the ESAT Laboratory of KU Leuven, in the frame of Fonds de la Recherche Scientifique—FNRS and Fonds Wetenschappelijk Onderzoek—Vlaanderen EOS Project under Grant 30452698; in part by the "(MUSE-WINET) Multi-Service Wireless Network," through Research Project FWO under Grant G.0B1818N; in part by the "Real-Time Adaptive Cross-Layer Dynamic Spectrum Management for Fifth Generation Broadband Copper Access Networks," through VLAIO O&O Project under Grant HBC.2017.1007; and in part by the "(MIA) Multi-Gigabit Innovations in Access."

ABSTRACT Recently, long reach x-digital subscriber line (LR-xDSL) has been proposed to extend the reach of conventional DSL systems. The extended loop lengths are characterized by a longer channel impulse response (CIR), which requires a similarly longer cyclic prefix (CP) to successfully eliminate the inter-symbol interference (ISI) between successive time-domain discrete multi-tone (DMT) symbols and inter-carrier interference (ICI) between the carriers or tones of the same DMT symbol. This adds a large overhead to the transmitted symbols and results in throughput loss. A per-tone equalizer (PTEQ) is an attractive alternative to deal with extended loop lengths. However, it imposes a large initialization computational complexity and memory requirement, hindering the use of a PTEQ in practical multiple-input multiple-output (MIMO) scenarios. To tackle this problem, a specific structure in the MIMO DSL channel, namely that the combined ISI and ICI signal power from the crosstalk channels is significantly lower than the desired and combined ISI and ICI signal power from the direct channels, may be exploited in deriving a novel low complexity/memory solution, here referred as sparse MIMO PTEQ, with negligible impact ($\approx$ 0.5% drop) on performance compared to a full MIMO PTEQ. For a conventional DSL binder size of 16 lines and a PTEQ order of 3, the proposed sparse MIMO PTEQ performs at 42% of the initialization computational complexity and 29.7% of the memory requirement, with negligible performance degradation, compared to a full MIMO PTEQ. The initialization computational complexity and memory requirement is further reduced by the proposed diagonal MIMO PTEQ which operates at 0.4% of the initialization computational complexity of a full MIMO PTEQ and requires 6.25% memory compared to a full MIMO PTEQ, with some degradation in the performance compared to the full MIMO PTEQ. The diagonal MIMO PTEQ has the additional benefit that it can be applied in both upstream and downstream scenarios, in contrast to the full and sparse MIMO PTEQ which can be used only in upstream scenarios.

INDEX TERMS DMT, long reach xDSL, MIMO per-tone equalizer, MIMO DSL systems, OFDM.

I. INTRODUCTION

DIGITAL subscriber line (DSL) technologies hold a major market-share of broadband communication [1]. They are based on discrete multi-tone (DMT) modulation, which is a multicarrier modulation technique similar to orthogonal frequency division multiplexing (OFDM). DMT is used in wireline communication, where channels are slowly time-varying and the noise in the channel is assumed stationary. Hence channels are assumed to be known after an initial training and quasi-static. This allows DMT to use bit-loading and adaptive power loading in addition to basic OFDM operation. In DMT on the transmitter side, the input bits to be transmitted are converted into parallel bit streams, each stream to be carried on a carrier or tone (a discrete

sub-band in the available bandwidth). In each stream, the bits are converted into higher order QAM symbols (up to 16384-QAM [2]), which are then modulated on to the discrete tones by an inverse discrete Fourier transform (IDFT) operation to obtain time-domain symbols. A cyclic prefix (CP) is added which—provided that its length at least matches the length of the channel impulse response (CIR), and the transmitter and receiver are properly synchronized—eliminates inter-symbol interference (ISI) between successive time-domain DMT symbols and inter-carrier interference (ICI) between the tones of the same DMT symbol. On the receiver side, the CP is removed from the received time-domain symbols and subsequently a discrete Fourier transform (DFT) is applied. Finally, the received QAM symbols are equalized with a single-tap complex frequency-domain equalizer (FEQ).

In an ideal scenario, the combination of CP and FEQ works perfectly to counter ISI and ICI. In older generations of DSL, such as ADSL [3] (and its later versions ADSL2 and ADSL2+), the allowed loop lengths ranged up to 5000 meters and the available channel bandwidth ranged up to only a few MHz. Hence, these older generations have been characterized by a long CIR and low crosstalk levels enabling a per-line single-input single-output (SISO) design. Although the use of a similarly long CP eliminates ISI and ICI, it also increases the DMT symbol length, thereby introducing an overhead and decreasing the achievable throughput. An efficient way to deal with this problem has been the use of a channel shortening filter—commonly known as a time-domain equalizer (TEQ) [4]. However in later generations of DSL (e.g., VDSL2 [5], G.fast [6], G.mgfast [7]) the copper loop lengths have been effectively shortened with the deployment of fibre to the distribution point unit (DPU), The typical loop lengths for VDSL2, G.fast and G.mgfast are 1200m, 250m and 100m, respectively. Hence, channel shortening has not been used in the later generations of DSL, confining its use to ADSL.

Recently long reach VDSL2 (LR-VDSL2) has been proposed with the purpose of providing high data rates (possibly up to $40 Mbit/s$ for downstream [8]) and a longer reach than conventional VDSL2 (up to 2100m) for areas where optical fibre cannot easily be deployed (due to geographical or financial barriers) [9]. Hence, the need for transmitting data over longer loops again motivates the use of a TEQ for LR-VDSL2. Moreover, long reach G.fast (LR-G.fast) is also being considered (within Q4/15 ITU standardization). A recent use case proposed under Q4/15 ITU standardization is for G.mgfast, which is arguably also the last DSL standard. In G.mgfast deployment, one of the proposed scenarios is a dual mode DPU, to serve G.mgfast for shorter loop lengths and G.fast and LR-G.fast for longer loop lengths.

These long reach extensions of existing DSL standards (LR-xDSL) will enable VDSL2 and G.fast DPUs to be connected to lines with a wider variety of lengths. All the lines connected to the same DPU have to use the same CP length in order to simplify the system and allow for efficient vectoring. If the CP length is chosen according to the longest line length then shorter lines may undergo a substantial throughput loss in order to enable ISI/ICI-free transmission on the longer lines, further motivating the use of a TEQ for LR-xDSL. However, since crosstalk can no longer be neglected in VDSL2 and later generations of DSL, a multiple-input multiple-output (MIMO) TEQ design is required for a joint shortening of both direct and crosstalk channels. Nevertheless, in the case of LR-VDSL2, besides ISI/ICI, there is an additional issue of echo and near-end crosstalk (NEXT) generation when considering a too short CP. This can be partly solved by echo cancellation techniques [10]–[12]. Moreover, it is emphasized that the main application use-case of the paper is LR-G.fast, in which this issue of NEXT and echo does not appear. For ISI/ICI cancellation with short CP, the MIMO TEQ has been shown to do a fairly good job in terms of shortening the CIRs [9]. However, the TEQ design procedure is generally not related to true bitrate optimization of the system. Therefore, a good TEQ in terms of the channel shortening, may indeed not guarantee a corresponding significant improvement in bitrates. In [13], a SISO bitrate maximizing TEQ (BM-TEQ) has been proposed to maximize the total bitrate for a given filter order, but this comes with a large initialization computational complexity due to a non-linear non-convex cost function. Similarly, in [14], [15] a genetic algorithm based blind channel shortening equalizer structure has been proposed, for the optimal SISO TEQ coefficients search. However again, a large initialization computational complexity is incurred. Moreover, the bitrate achieved by a TEQ is known to be sensitive to the synchronization delay and their relation is non-smooth [16].

A MIMO per-tone equalizer (PTEQ) [17], [18] provides a solution to these problems faced by a MIMO TEQ. In a MIMO PTEQ, the TEQ is moved to after the DFT operations at the receiver side. Hence, each tone has its own filter, designed to maximize the signal-to-noise ratio (SNR) by solving a minimum mean squared error (MMSE) problem for each tone separately. Not only does a PTEQ provide an upper limit to the performance of a TEQ, it also yields a relation between SNR and synchronisation delay that is smooth and predictable [18], thereby simplifying determining the optimal synchronization delay. Furthermore, it has been shown that the runtime computational complexity of the MIMO PTEQ is equal or less than the runtime computational complexity of a MIMO TEQ [18]. Moreover, recently in [19] a transmitter side per-tone precoder has been proposed, which can be applied at the DPU in a downstream scenario, thus reducing the computational load on customer-premises equipment (CPE). Finally, apart from ISI/ICI cancellation, the MIMO PTEQ also performs crosstalk cancellation, removing the need for a separate entity (vectoring) for crosstalk cancellation [20]–[22].

A. MAIN CONTRIBUTIONS

Despite the advantages of the MIMO PTEQ, a large initialization computational complexity and memory requirement hinder its applicability in practical scenarios. To tackle this

problem, a specific structure in the MIMO DSL channel, namely that the combined ISI and ICI signal power from the crosstalk channels is significantly lower than the desired and combined ISI and ICI signal power from the direct channels, is exploited in deriving two new MIMO PTEQ structures, that reduce the initialization computational complexity and memory requirement of a full MIMO PTEQ. The two proposed structures are the sparse MIMO PTEQ and diagonal MIMO PTEQ.

(*i*) The proposed sparse MIMO PTEQ results in negligible loss of performance. From the simulation results obtained in Section VII it is observed that for an order-1 full MIMO PTEQ and an order-1 sparse MIMO PTEQ, the average difference in achieved data rate, over all synchronization delays, is only $\approx 0.5\%$. The average difference in the peak data rate is only $\approx 0.1\%$.

(*ii*) The proposed diagonal MIMO PTEQ results a in further reduction of the initialization computational complexity, runtime computational complexity and memory requirement at the cost of a small performance loss. The diagonal MIMO PTEQ has the additional benefit that it can be applied in both upstream and downstream scenarios, in contrast to the full and sparse MIMO PTEQ structures which can be used only in upstream scenarios.

A similar reduction in the initialization computational complexity and memory requirement has been proposed for the MIMO TEQ in [9]. The basic ideas proposed in this paper and in [9] are similar in that both papers aim at reducing the computational complexity and memory requirement, for MIMO PTEQ and MIMO TEQ, respectively. However, the MIMO TEQ, discussed in [9], aims at channel shortening while the MIMO PTEQ aims at bit rate maximization. Therefore, the underlying system equations, constrained optimization problems and cost functions are very different in the two papers.

B. ORGANIZATION AND NOTATION

The paper is organized as follows: Section II provides a brief overview of the MIMO DSL system model and reviews the full MIMO PTEQ design equations. Section III and Section IV present the sparse and diagonal MIMO PTEQ structure, respectively. Section V and Section VI present the initialization computational complexity and memory requirement of proposed MIMO PTEQ structures, respectively. Section VII reports the results and finally Section VIII concludes the paper.

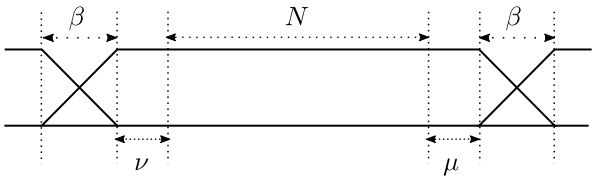

FIGURE 1. Time-domain transmitted symbol for xDSL.

Lower-case and upper-case boldface letters are used to denote vectors (row vectors and column vectors) and matrices, respectively, with $\mathbf{a}_{l:m}$ representing elements of vector $\mathbf{a}$ with indices from l to m. Further, $(.)^T$ is used to represent the transpose operation, $(.)^H$ the Hermitian transpose operation, $(.)^*$ complex conjugation and $\mathbb{E}[.]$ the expected value operation.

II. MIMO PTEQ

The system considered is a cable binder with M lines (users) corresponding to an $M \times M$ baseband communication system with additive white Gaussian noise and time-dispersive channels of length L. In VDSL2 and later generations of DSL, transmit pulse shaping is also applied to the DMT symbols to reduce the effect of echo and near-end crosstalk (NEXT) [23]. A CP of length $\nu+\beta$ and a cyclic suffix (CS) of length $\mu+\beta$ are then added to the DMT symbol of size N (N represents the IDFT (DFT) size used at the transmitter (receiver)). A transmit pulse shaping with a window (usually a raised-cosine window) with roll-off length of β is applied to both ends of the symbol and eventually successive symbols are overlapped with an overlap length of β, as shown in Fig. 1.

Hence, the time-domain received signal for user $m = 1, \ldots, M$ is given in (1), shown at the bottom of the page. Here, T is the equalizer length, s denotes the symbol period after the overlapping of successive symbols, given by

$$\underbrace{\begin{bmatrix} y^m_{ks+\nu-T+2} \\ \vdots \\ y^m_{ks+\nu+N-1} \\ y^m_{ks+\nu+N} \end{bmatrix}}_{\mathbf{y}^m_{[k]}} = \sum_{j=1}^{M} \underbrace{\left[\begin{array}{c|cccccc|c} \mathbf{O_1} & h^{ml}_{L-1} & \cdots & h^{ml}_0 & 0 & \cdots & \\ & 0 & h^{ml}_{L-1} & \cdots & h^{ml}_0 & \cdots & \\ & \vdots & \ddots & \ddots & \ddots & 0 & \mathbf{O_2} \\ & 0 & \cdots & h^{ml}_{L-1} & \cdots & h^{ml}_0 & \end{array}\right] \begin{bmatrix} \mathbf{I} & & \\ & \mathbf{I} & \\ & & \mathbf{I} \end{bmatrix}}_{\mathbf{H}^{ml}} \begin{bmatrix} \mathbf{C} & \mathbf{0} & \mathbf{0} \\ \mathbf{0} & \mathbf{C} & \mathbf{0} \\ \mathbf{0} & \mathbf{0} & \mathbf{C} \end{bmatrix} \begin{bmatrix} \mathbb{I}_N & \mathbf{0} & \mathbf{0} \\ \mathbf{0} & \mathbb{I}_N & \mathbf{0} \\ \mathbf{0} & \mathbf{0} & \mathbb{I}_N \end{bmatrix} \underbrace{\begin{bmatrix} \ddot{\mathbf{x}}^l_{(k-1)} \\ \ddot{\mathbf{x}}^l_{(k)} \\ \ddot{\mathbf{x}}^l_{(k+1)} \end{bmatrix}}_{\ddot{\mathbf{x}}^l_{[k]}} + \underbrace{\begin{bmatrix} n^m_{ks+\nu-T+2} \\ \vdots \\ n^m_{ks+\nu+N-1} \\ n^m_{ks+\nu+N} \end{bmatrix}}_{\mathbf{n}^m_{[k]}}$$

$$\implies \mathbf{y}^m_{[k]} = \sum_{l=1}^{M} \mathbf{H}^{ml} \ddot{\mathbf{x}}^l_{[k]} + \mathbf{n}^m_{[k]} \tag{1}$$

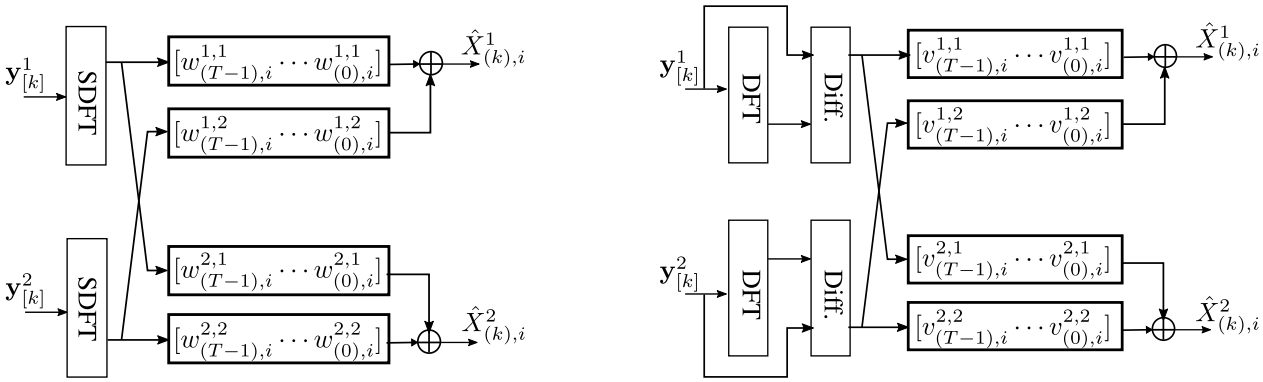

(a) Full MIMO PTEQ with sliding DFT

(b) Full MIMO PTEQ with single DFT and difference terms

FIGURE 2. Block diagram of 2x2 full MIMO PTEQ.

$s = N + \nu + \mu + \beta$. Vector $\ddot{\mathbf{x}}^l_{(k)} \triangleq \left[X^l_{(k),1}, X^l_{(k),2} \cdots X^l_{(k),N}\right]^T$ represents the k^{th} symbol of user l, with $X^l_{(k),i}$ the QAM-symbol for tone $i = 1, \ldots, N$. Matrix $\mathbb{I}_N$ is an $N \times N$ IDFT matrix. Matrix $\mathbf{C}$ adds the CS and CP to the symbols and performs transmit pulse shaping. The structure of the matrix $\mathbf{C}$ is as follows

$$\mathbf{C} = \left[\begin{array}{cc|c} \mathbf{0} & \mathbf{0} & \mathbf{C}_1 \\ \hline & \mathbf{I}_N & \\ \hline \mathbf{C}_2 & \mathbf{0} & \mathbf{0} \end{array}\right] \tag{2a}$$

$$\mathbf{C}_1 = \left[\begin{array}{c|c} \mathbf{I}_\beta \mathrm{diag}\left(\boldsymbol{\varpi}_{1:\beta}\right) & \mathbf{0}_{\beta\times\nu} \\ \hline \mathbf{0}_{\nu\times\beta} & \mathbf{I}_\nu \end{array}\right] \tag{2b}$$

$$\mathbf{C}_2 = \left[\begin{array}{c|c} \mathbf{I}_\mu & \mathbf{0}_{\mu\times\beta} \\ \hline \mathbf{0}_{\beta\times\mu} & \mathbf{I}_\beta \mathrm{diag}(\boldsymbol{\varpi}_{\beta:end}) \end{array}\right] \tag{2c}$$

where, $\boldsymbol{\varpi}$ is the raised cosine window given as

$$\boldsymbol{\varpi}_l = \frac{1}{2}\left[1 + cos\left(\frac{\pi}{\beta}(l-\beta)\right)\right] \quad 1 \le l \le 2\beta \tag{3}$$

The $\boxed{\mathbf{I}}$ in formula (1) represents an identity matrix of dimension $N + \nu + \mu + 2\beta$ which in the compound matrix has β rows overlap with the next and/or previous $\boxed{\mathbf{I}}$. Finally, h^{ml}_j, which is a part of channel matrix $\mathbf{H}^{ml}$, represents the j^{th} tap of the channel from user l to user m, and $\mathbf{O_1}$ and $\mathbf{O_2}$ are all-zero matrices with dimensions $(N+T-1) \times (N+2\nu+\mu+2\beta-L-T+2+\Delta)$ and $(N+T-1) \times (N+\nu+2\mu+2\beta-\Delta)$ receptively, where Δ is the so-called synchronization delay—a design parameter. For ease of notation we do not include Δ in the system equations and variables, from here on.

The MIMO PTEQ, as described in [18], is an $M \times M$ equalizer of length T (order $T-1$), applied to the output of a sliding DFT (SDFT) of the received signals $\mathbf{y}^m_{[k]}$ (Fig. 2(a)), i.e.,

$$\ddot{\mathbf{y}}^m_{[k],i} = \mathbf{F}_i \; \mathbf{y}^m_{[k]} \tag{4}$$

where $\ddot{\mathbf{y}}^m_{[k],i}$ is the $T \times 1$ SDFT output for user m on tone i, with

$$\mathbf{F}_i = \begin{bmatrix} \boxed{\mathrm{row}_i(\mathbb{F}_\mathbf{N})} & \cdots & 0 \\ 0 \; \boxed{\mathrm{row}_i(\mathbb{F}_\mathbf{N})} & \cdots & 0 \\ \vdots & \ddots & \vdots \\ 0 \quad \cdots & & \boxed{\mathrm{row}_i(\mathbb{F}_\mathbf{N})} \end{bmatrix} \tag{5}$$

where $\mathbb{F}_\mathbf{N}$ is an $N \times N$ DFT matrix and $\mathrm{row}_i(\mathbb{F}_\mathbf{N})$ represents the i^{th} row of the DFT matrix $\mathbb{F}_\mathbf{N}$. These SDFT outputs on tone i can be combined for all users in a single $MT \times 1$ vector

$$\underbrace{\begin{bmatrix} \ddot{\mathbf{y}}^1_{[k],i} \\ \ddot{\mathbf{y}}^2_{[k],i} \\ \vdots \\ \ddot{\mathbf{y}}^M_{[k],i} \end{bmatrix}}_{\ddot{\mathbf{y}}_{[k],i}} = \underbrace{\begin{bmatrix} \mathbf{F}_i & \mathbf{0} & \cdots & \mathbf{0} \\ \mathbf{0} & \mathbf{F}_i & \cdots & \mathbf{0} \\ \vdots & \ddots & \ddots & \vdots \\ \mathbf{0} & \cdots & \cdots & \mathbf{F}_i \end{bmatrix}}_{\breve{\mathbf{F}}_i} \underbrace{\begin{bmatrix} \mathbf{y}^1_{[k]} \\ \mathbf{y}^2_{[k]} \\ \vdots \\ \mathbf{y}^M_{[k]} \end{bmatrix}}_{\mathbf{y}_{[k]}} \tag{6}$$

The aim of a MIMO PTEQ is to generate an estimate of the k^{th} transmitted symbol ($X^m_{(k),i}$) from the SDFT output vector on tone i ($\ddot{\mathbf{y}}_{[k],i}$), for all the users m and tones i. Hence, the estimated k^{th} transmitted symbol for user m on tone i, with the full MIMO PTEQ, is given as

$$\hat{X}^m_{(k),i} = \mathbf{w}^m_i \ddot{\mathbf{y}}_{[k],i} \tag{7}$$

Here, $\mathbf{w}^m_i$ contains the MIMO PTEQ coefficients for user m on tone i, i.e.,

$$\mathbf{w}^m_i = \begin{bmatrix} \mathbf{w}^{m1}_i & \mathbf{w}^{m2}_i & \cdots & \mathbf{w}^{mm}_i & \cdots & \mathbf{w}^{mM}_i \end{bmatrix} \tag{8}$$

where, each $\mathbf{w}^{ml}_i$ represents an equalizer of order $T-1$:

$$\mathbf{w}^{ml}_i = \begin{bmatrix} w^{ml}_{(T-1),i} & w^{ml}_{(T-2),i} & \cdots & w^{ml}_{(0),i} \end{bmatrix} \tag{9}$$

These MIMO PTEQ coefficients for tone i can be stacked for all users in a single matrix, yielding a full MIMO PTEQ matrix for tone i

$$\mathbf{W}_i = \begin{bmatrix} \mathbf{w}^{11}_i & \mathbf{w}^{12}_i & \cdots & \mathbf{w}^{1M}_i \\ \mathbf{w}^{21}_i & \mathbf{w}^{22}_i & \cdots & \mathbf{w}^{2M}_i \\ \vdots & & \ddots & \\ \mathbf{w}^{M1}_i & \mathbf{w}^{M2}_i & \cdots & \mathbf{w}^{MM}_i \end{bmatrix} \tag{10}$$

Using (1), the estimated k^{th} transmitted symbol for user m on tone i, (7) can be rewritten as

$$\hat{X}^m_{(k),i} = \mathbf{w}^m_i \breve{\mathbf{F}}_i \left(\begin{bmatrix} \mathbf{H}^{11} & \mathbf{H}^{12} & \cdots & \mathbf{H}^{1M} \\ \mathbf{H}^{21} & \mathbf{H}^{22} & \cdots & \mathbf{H}^{2M} \\ \vdots & \vdots & \cdots & \vdots \\ \mathbf{H}^{M1} & \mathbf{H}^{M2} & \cdots & \mathbf{H}^{MM} \end{bmatrix} \begin{bmatrix} \breve{\mathbf{x}}^1_{[k]} \\ \breve{\mathbf{x}}^2_{[k]} \\ \vdots \\ \breve{\mathbf{x}}^M_{[k]} \end{bmatrix} + \begin{bmatrix} \mathbf{n}^1_{[k]} \\ \mathbf{n}^2_{[k]} \\ \vdots \\ \mathbf{n}^M_{[k]} \end{bmatrix} \right) \tag{11}$$

Based on (5) and (6), it can be observed that MT DFT operations are required to generate $\ddot{\mathbf{y}}_{[k],i}$, leading to a large runtime computational complexity. However, in [17], a more efficient difference terms based implementation of the SDFT for the PTEQ has been proposed as follows. The SDFT matrix $\mathbf{F}_i$ can be decomposed [19] into a lower triangular matrix and a sparse matrix, i.e.,

$$\mathbf{F}_i = \underbrace{\begin{bmatrix} \alpha^{0i} & \cdots & 0 \\ \vdots & \ddots & \vdots \\ \alpha^{(T-1)i} & \cdots & \alpha^{0i} \end{bmatrix}}_{\mathbf{L}_i} \underbrace{\left[\begin{array}{c|c} \text{row}_i(\mathbb{F}_\mathbf{N}) & \mathbf{0} \\ \hline -\alpha^i \mathbf{I}_{T-1} \quad \mathbf{0} & \alpha^i \mathbf{I}_{T-1} \end{array}\right]}_{\underline{\mathrm{F}}_i} \tag{12}$$

where $\alpha = \exp^{-j2\pi/N}$. The first row of the matrix $\underline{\mathrm{F}}_i$ corresponds to a single DFT operation and the other rows result in $T-1$ so-called difference terms. Hence, utilizing the difference terms implementation instead of the SDFT, (7) can be rewritten as

$$\hat{X}^m_{(k),i} = \mathbf{v}^m_i \underline{\breve{\mathrm{F}}}_i \mathbf{y}_{[k]} \tag{13}$$

where $\underline{\breve{\mathrm{F}}}_i$ is given as

$$\underline{\breve{\mathrm{F}}}_i = \begin{bmatrix} \underline{\mathrm{F}}_i & \mathbf{0} & \cdots & \mathbf{0} \\ \mathbf{0} & \underline{\mathrm{F}}_i & \cdots & \mathbf{0} \\ \vdots & \ddots & \ddots & \vdots \\ \mathbf{0} & \cdots & \cdots & \underline{\mathrm{F}}_i \end{bmatrix} \tag{14}$$

and $\mathbf{v}^m_i$ are the modified PTEQ coefficients with $\mathbf{v}^{m,l}_i = \mathbf{L}^T_i \mathbf{w}^{m,l}_i$, which will then be computed directly instead of the original PTEQ coefficients $\mathbf{w}^m_i$. Similar to $\mathbf{W}_i$ in (10), the full MIMO PTEQ matrix for tone i with modified PTEQ coefficients $\mathbf{v}^m_i$ can be written as

$$\mathbf{V}_i = \begin{bmatrix} \mathbf{v}^{11}_i & \mathbf{v}^{12}_i & \cdots & \mathbf{v}^{1M}_i \\ \mathbf{v}^{21}_i & \mathbf{v}^{22}_i & \cdots & \mathbf{v}^{2M}_i \\ \vdots & & \ddots & \\ \mathbf{v}^{M1}_i & \mathbf{v}^{M2}_i & \cdots & \mathbf{v}^{MM}_i \end{bmatrix} \tag{15}$$

where, each $\mathbf{v}^{ml}_i$ represents an equalizer of order $T-1$:

$$\mathbf{v}^{ml}_i = \begin{bmatrix} v^{ml}_{(T-1),i} & v^{ml}_{(T-2),i} & \cdots & v^{ml}_{(0),i} \end{bmatrix} \tag{16}$$

Finally, the optimization problem for the optimal (MMSE based) full MIMO PTEQ filter coefficients for user m on tone i is defined as

$$\begin{aligned} &\underset{\mathbf{v}^\mathbf{m}_\mathbf{i}}{\text{minimize}} \quad \mathbb{E}\left[\left| \hat{X}^m_{(k),i} - X^m_{(k),i} \right|^2 \right] \\ &\qquad (or) \\ &\underset{\mathbf{v}^\mathbf{m}_\mathbf{i}}{\text{minimize}} \quad \mathbb{E}\left[\left| \mathbf{v}^m_i \underline{\breve{\mathrm{F}}}_i \mathbf{y}_{[k]} - X^m_{(k),i} \right|^2 \right] \end{aligned} \tag{17}$$

where, the latter can be obtained from the former by substituting the definition of $\hat{X}^m_{(k),i}$ from (13). The solution to the optimization problem (17) is given by (see Appendix)

$$\left(\tilde{\mathbf{v}}^m_i\right)^H = \mathbb{E}\left[\ddot{\mathbf{y}}_{[k],i} \left(\ddot{\mathbf{y}}_{[k],i} \right)^H \right]^{-1} \mathbb{E}\left[\ddot{\mathbf{y}}_{[k],i} \left(X^m_{(k),i} \right)^* \right] \tag{18}$$

The solution can be further written as a function of the channel matrices, input correlation and noise correlation matrices, based on (1). This is left out here for conciseness (see also Sections III and IV for similar derivations).

Furthermore, it is to be noticed that if the CP length is too short, the received signals after the DMT demodulation (before a soft/hard decision operation) are generally improper [24], [25]. However, [26] proposed a widely-linear PTEQ (WL-PTEQ) considering impropriety of the received signals and observed that the achieved bitrates for various CP lengths (shorter than CIR) roughly coincide for the PTEQ and WL-PTEQ for equalizer order greater than 0. Therefore, this paper ignores the impropriety of the received signals after DMT demodulation.

III. SPARSE MIMO PTEQ

The full MIMO PTEQ design described in Section II thus circumvents the difficult bitrate maximizing MIMO TEQ design: The minimization in (17) directly corresponds to the maximization of the achievable bitrate for user m on tone i [17], [18]. However, despite the advantages of the MIMO PTEQ, its large initialization computational complexity and memory requirement hinder its applicability in practical scenarios. In this section, a first solution to this problem is proposed with a sparse MIMO PTEQ.

For MIMO DSL systems (without a TEQ/PTEQ), the combined ISI and ICI signal power from the crosstalk channels is negligible compared to the desired and the combined ISI and ICI power from the direct channels. Fig. 3 shows this structure for a 2×2 MIMO DSL system (without a TEQ/PTEQ) where the CP is shorter than the CIR (no CS is used here). The desired signal power and combined ISI and ICI power, contributed by measured dispersive DSL channels, are calculated [27] and plotted for both direct channels and crosstalk channels. It can be further observed that the combined ISI and ICI signal power from the direct channels is comparable and past a certain frequency even higher than the desired signal power from the direct channels. Thus, a multi-taps equalizer, represented by the diagonal elements of MIMO PTEQ matrix is used to combat the combined ISI and ICI signal power from the direct channels.

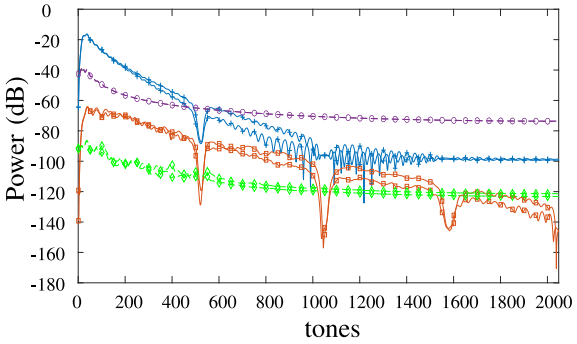

(a) Power distribution for measured channel 1

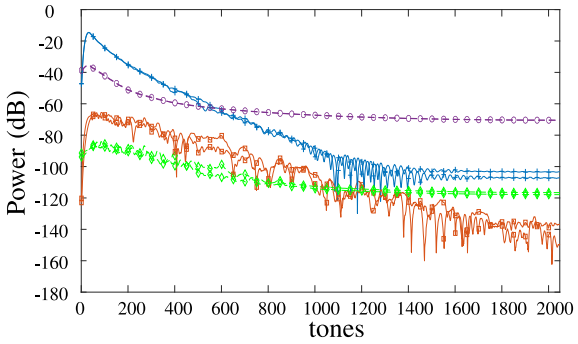

(b) Power distribution for measured channel 2

FIGURE 3. Power distribution as desired signal power and combined ISI and ICI power for two measured 2 × 2 MIMO DSL channels by two Tier-1 operators. Desired signal power from direct channels (—+—), combined ISI and ICI signal power from direct channels (– ⊖ –), desired signal power from crosstalk channels (—□—), combined ISI and ICI signal power from crosstalk channels (– ◇ –).

However, comparatively, the combined ISI and ICI signal power from the crosstalk channels is negligible, especially in the lower frequencies, which is generally the high SNR region in DSL systems and hence contributes most to the data rate. Therefore, this structure can be exploited to significantly simplify the full MIMO PTEQ without impacting the performance, namely by reducing the MIMO PTEQ coefficients responsible for crosstalk ISI and ICI cancellation to a single tap scalar. The sparse MIMO PTEQ matrix elements for tone i are then defined as

$$\begin{aligned}\mathbf{v}_i^{ml} &= \begin{bmatrix} v_{(T-1),i}^{ml} & v_{(T-2),i}^{ml} & \cdots & v_{(0),i}^{ml} \end{bmatrix} \quad \forall m = l \\ \mathbf{v}_i^{ml} &= \begin{bmatrix} v_{(0),i}^{ml} & 0 & \cdots & 0 \end{bmatrix} \equiv v_i^{ml}\underline{\mathbf{e}} \quad \forall m \neq l \end{aligned} \tag{19}$$

where $\underline{\mathbf{e}} = [1\ 0\ 0\ \cdots\ 0]_{1\times T}$. Hence, the sparse MIMO PTEQ coefficients for user m on tone i are given as

$$\mathbf{v}_i^m = \begin{bmatrix} v_i^{m1}\underline{\mathbf{e}} & v_i^{m2}\underline{\mathbf{e}} & \cdots & \mathbf{v}_i^{mm} & \cdots & v_i^{mM}\underline{\mathbf{e}} \end{bmatrix} \tag{20}$$

and the sparse MIMO PTEQ matrix for tone i is given as

$$\mathbf{V}_i = \begin{bmatrix} \mathbf{v}_i^{11} & v_i^{12}\underline{\mathbf{e}} & \cdots & v_i^{1M}\underline{\mathbf{e}} \\ v_i^{21}\underline{\mathbf{e}} & \mathbf{v}_i^{22} & \cdots & v_i^{2M}\underline{\mathbf{e}} \\ \vdots & & \ddots & \\ v_i^{M1}\underline{\mathbf{e}} & v_i^{M2}\underline{\mathbf{e}} & \cdots & \mathbf{v}_i^{MM} \end{bmatrix} \tag{21}$$

The estimated k^{th} transmitted symbol for user m on tone i, with the sparse MIMO PTEQ is given as

$$\hat{X}_{(k),i}^m = \mathbf{v}_i^m \check{\underline{\mathbf{F}}}_i \mathbf{y}_{[k]} \tag{22}$$

which, using (20) and (14), is equivalent to (23), shown at the bottom of the page, where, $\check{\underline{\mathbf{F}}}_i^m$ now has $T+M-1$ rows (compared to MT rows for $\check{\underline{\mathbf{F}}}_i$ in (13)).

Hence the MMSE based optimization problem for the sparse MIMO PTEQ filter coefficients for user m on tone i is given as

$$\underset{\tilde{\mathbf{v}}_i^{\mathbf{m}}}{\text{minimize}} \quad \mathbb{E}\left[\left|\tilde{\mathbf{v}}_i^m \check{\underline{\mathbf{F}}}_i^m \mathbf{y}_{[k]} - X_{(k),i}^m\right|^2\right] \tag{24}$$

Denoting $\mathring{\mathbf{y}}_{[k],i}^m = \check{\underline{\mathbf{F}}}_i^m \mathbf{y}_{[k]}$. The solution to the optimization problem (24) is given by

$$\left(\tilde{\mathbf{v}}_i^m\right)^H = \left(\mathbb{E}\left[\mathring{\mathbf{y}}_{[k],i}^m \left(\mathring{\mathbf{y}}_{[k],i}^m\right)^H\right]\right)^{-1} \left(\mathbb{E}\left[\mathring{\mathbf{y}}_{[k],i}^m \left(X_{(k),i}^m\right)^*\right]\right) \tag{25}$$

The solution can be further written as a function of the channel matrices, input correlation and noise correlation matrices. The first part of (25) ($\mathbb{E}[\mathring{\mathbf{y}}_{[k],i}^m(\mathring{\mathbf{y}}_{[k],i}^m)^H]$) can be expanded as

$$\begin{aligned}\mathbb{E}\left[\mathring{\mathbf{y}}_{[k],i}^m \left(\mathring{\mathbf{y}}_{[k],i}^m\right)^H\right] &= \check{\underline{\mathbf{F}}}_i^m \mathbb{E}\left[\begin{bmatrix} \mathbf{y}_{[k]}^1 \\ \mathbf{y}_{[k]}^2 \\ \vdots \\ \mathbf{y}_{[k]}^M \end{bmatrix} \begin{bmatrix} \mathbf{y}_{[k]}^1 \\ \mathbf{y}_{[k]}^2 \\ \vdots \\ \mathbf{y}_{[k]}^M \end{bmatrix}^H\right] \check{\underline{\mathbf{F}}}_i^{mH} \\ &= \check{\underline{\mathbf{F}}}_i^m \mathbf{R}_{\mathbf{yy}} \check{\underline{\mathbf{F}}}_i^{mH} \end{aligned} \tag{26}$$

$$\hat{X}_{(k),i}^m = \underbrace{\begin{bmatrix} v_i^{m1} & \cdots & \mathbf{v}_i^{mm} & \cdots & v_i^{m1} \end{bmatrix}}_{\tilde{\mathbf{v}}_i^m} \underbrace{\begin{bmatrix} \boxed{\text{row}_i(\mathbb{F}_\mathbf{N})} & \mathbf{0} & \cdots & \cdots & \mathbf{0} & \cdots & \mathbf{0} \\ \vdots & \ddots & \ddots & \cdots & \ddots & \ddots & \vdots \\ \mathbf{0} & \cdots & \boxed{\text{row}_i(\mathbb{F}_\mathbf{N})} & \mathbf{0} & \cdots & \cdots & \mathbf{0} \\ \hline \mathbf{0} & \cdots & \cdots & \underline{\mathbf{F}}_i & \cdots & \cdots & \mathbf{0} \\ \hline \mathbf{0} & \cdots & \cdots & \mathbf{0} & \boxed{\text{row}_i(\mathbb{F}_\mathbf{N})} & \cdots & \mathbf{0} \\ \vdots & \ddots & \ddots & \cdots & \ddots & \ddots & \vdots \\ \mathbf{0} & \mathbf{0} & \cdots & \mathbf{0} & \cdots & \cdots & \boxed{\text{row}_i(\mathbb{F}_\mathbf{N})} \end{bmatrix}}_{\check{\underline{\mathbf{F}}}_i^m} \mathbf{y}_{[k]} \tag{23}$$

The output correlation matrix $\mathbf{R_{yy}}$ is given as

$$\mathbf{R_{yy}} = \begin{bmatrix} \mathbb{E}\left[\mathbf{y}^1_{[k]}\mathbf{y}^{1^H}_{[k]}\right] & \mathbb{E}\left[\mathbf{y}^1_{[k]}\mathbf{y}^{2^H}_{[k]}\right] & \cdots & \mathbb{E}\left[\mathbf{y}^1_{[k]}\mathbf{y}^{M^H}_{[k]}\right] \\ \mathbb{E}\left[\mathbf{y}^2_{[k]}\mathbf{y}^{1^H}_{[k]}\right] & \mathbb{E}\left[\mathbf{y}^2_{[k]}\mathbf{y}^{2^H}_{[k]}\right] & \cdots & \mathbb{E}\left[\mathbf{y}^2_{[k]}\mathbf{y}^{M^H}_{[k]}\right] \\ \vdots & \vdots & \cdots & \vdots \\ \mathbb{E}\left[\mathbf{y}^M_{[k]}\mathbf{y}^{1^H}_{[k]}\right] & \mathbb{E}\left[\mathbf{y}^M_{[k]}\mathbf{y}^{2^H}_{[k]}\right] & \cdots & \mathbb{E}\left[\mathbf{y}^M_{[k]}\mathbf{y}^{M^H}_{[k]}\right] \end{bmatrix} \tag{27}$$

which can be written as a function of the known input correlation and noise correlation matrices, assuming the noise on different lines are independent

$$\begin{aligned} \mathbb{E}\left[\mathbf{y}^p_{[k]}\mathbf{y}^{q^H}_{[k]}\right] &= \sum_{l=1}^{M} \mathbf{H}^{p,l}\mathbf{R}_{\check{\mathbf{x}}^l}\mathbf{H}^{q,l^H} \quad \forall p \neq q \\ \mathbb{E}\left[\mathbf{y}^p_{[k]}\mathbf{y}^{q^H}_{[k]}\right] &= \sum_{l=1}^{M} \mathbf{H}^{p,l}\mathbf{R}_{\check{\mathbf{x}}^l}\mathbf{H}^{q,l^H} + \mathbf{R}_{\mathbf{n}^p} \quad \forall p = q \end{aligned} \tag{28}$$

where, $\mathbf{R}_{\check{\mathbf{x}}^l}$ is the input symbols correlation matrix $\mathbf{R}_{\check{\mathbf{x}}^l} = \mathbb{E}[\check{\mathbf{x}}^l_{[k]}\check{\mathbf{x}}^{l^H}_{[k]}]$ and $\mathbf{R}_{\mathbf{n}^p}$ is the noise correlation matrix $\mathbf{R}_{\mathbf{n}^p} = \mathbb{E}[\mathbf{n}^p_{[k]}\mathbf{n}^{p^H}_{[k]}]$.

The second part of the (25) ($\mathbb{E}[\mathring{\mathbf{y}}^m_{[k],i}(X^m_{(k),i})^*]$) can be expanded as

$$\begin{aligned} \mathbb{E}\left[\mathring{\mathbf{y}}^m_{[k],i}\left(X^m_{(k),i}\right)^*\right] &= \mathbb{E}\left[\left(\underline{\check{\mathrm{F}}}^m_i \begin{bmatrix} \mathbf{y}^1_{[k]} \\ \mathbf{y}^2_{[k]} \\ \vdots \\ \mathbf{y}^M_{[k]} \end{bmatrix}\right)\left(X^m_{(k),i}\right)^*\right] \\ &= \mathbb{E}\left[\left(\underline{\check{\mathrm{F}}}^m_i \begin{bmatrix} \sum_{l=1}^{M} \mathbf{H}^{1l}\check{\mathbf{x}}^l_{[k]} + \mathbf{n}^1_{[k]} \\ \sum_{l=1}^{M} \mathbf{H}^{2l}\check{\mathbf{x}}^l_{[k]} + \mathbf{n}^2_{[k]} \\ \vdots \\ \sum_{l=1}^{M} \mathbf{H}^{Ml}\check{\mathbf{x}}^l_{[k]} + \mathbf{n}^M_{[k]} \end{bmatrix}\right)\left(\check{\mathbf{x}}^m_{[k]}\right)^H\mathbf{e}_i\right] \end{aligned} \tag{29}$$

where $\mathbf{e}_i = [0 \ \cdots \ 0 \ 1 \ 0 \ \cdots \ 0]^T_{1\times 3N}$, with the 1 in the $(N+i)^{th}$ position. Finally (29) can be rewritten as

$$\mathbb{E}\left[\mathring{\mathbf{y}}^m_{[k],i}\left(X^m_{(k),i}\right)^*\right] = \underline{\check{\mathrm{F}}}^m_i \begin{bmatrix} \mathbf{H}^{1m}\mathbf{R}_{\check{\mathbf{x}}^m}\mathbf{e}_i \\ \mathbf{H}^{2m}\mathbf{R}_{\check{\mathbf{x}}^m}\mathbf{e}_i \\ \vdots \\ \mathbf{H}^{Mm}\mathbf{R}_{\check{\mathbf{x}}^m}\mathbf{e}_i \end{bmatrix} \tag{30}$$

Thus, the optimal solution for sparse MIMO PTEQ coefficients for user m on tone i is given as (31), at the bottom of the next page.

IV. DIAGONAL MIMO PTEQ

A further reduction of the initialization computational complexity and memory requirement can be achieved by considering a diagonal MIMO PTEQ. In addition to achieving a reduction in the initialization computational complexity and memory requirement, a diagonal MIMO PTEQ can also be used in downstream scenarios, where no receiver coordination is possible. The diagonal MIMO PTEQ matrix elements

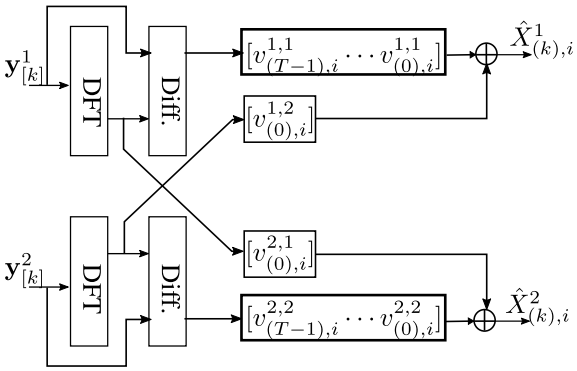

FIGURE 4. 2x2 sparse MIMO PTEQ for tone *i*.

for tone i are then defined as

$$\begin{aligned} \mathbf{v}^{ml}_i &= \begin{bmatrix} v^{ml}_{(T-1),i} & v^{ml}_{(T-2),i} & \cdots & v^{ml}_{(0),i} \end{bmatrix} \quad \forall m = l \\ \mathbf{v}^{ml}_i &= [\mathbf{0}]_{1\times T} \quad \forall m \neq l \end{aligned} \tag{32}$$

Hence, the diagonal MIMO PTEQ coefficients for user m on tone i are given as

$$\mathbf{v}^m_i = \begin{bmatrix} \mathbf{0} & \mathbf{0} & \cdots & \mathbf{v}^{mm}_i & \cdots & \mathbf{0} \end{bmatrix} \tag{33}$$

and the diagonal MIMO PTEQ matrix for tone i is given as

$$\mathbf{V}_i = \begin{bmatrix} \mathbf{v}^{11}_i & \mathbf{0} & \cdots & \mathbf{0} \\ \mathbf{0} & \mathbf{v}^{22}_i & \cdots & \mathbf{0} \\ \vdots & & \ddots & \\ \mathbf{0} & \mathbf{0} & \cdots & \mathbf{v}^{MM}_i \end{bmatrix} \tag{34}$$

The estimated k^{th} transmitted symbol for user m on tone i, with the diagonal MIMO PTEQ is given as

$$\hat{X}^m_{(k),i} = \mathbf{v}^m_i \underline{\check{\mathrm{F}}}_i \mathbf{y}_{[k]} \tag{35}$$

which, using (33) and (14) is equivalent to

$$\begin{aligned} \hat{X}^m_{(k),i} &= \mathbf{v}^{mm}_i \underline{\mathrm{F}}_i \mathbf{y}^m_{[k]} \\ &= \mathbf{v}^{mm}_i \underline{\mathrm{F}}_i \left(\begin{bmatrix} \mathbf{H}^{m1}\mathbf{H}^{m2}\cdots\mathbf{H}^{mM} \end{bmatrix}\begin{bmatrix} \check{\mathbf{x}}^1_{[k]} \\ \check{\mathbf{x}}^2_{[k]} \\ \vdots \\ \check{\mathbf{x}}^M_{[k]} \end{bmatrix} + \mathbf{n}^m_{[k]}\right) \end{aligned} \tag{36}$$

where $\underline{\mathrm{F}}_i$ has T rows (compared to $T+M-1$ rows for $\underline{\check{\mathrm{F}}}^m_i$ in (23)). Similar to (24), the MMSE based optimization problem for the diagonal PTEQ filter coefficients for user m on tone i is given as

$$\underset{\mathbf{v}^{mm}_i}{\text{minimize}} \quad \mathbb{E}\left[\left|\mathbf{v}^{mm}_i \underline{\mathrm{F}}_i \mathbf{y}^m_{[k]} - X^m_{(k),i}\right|^2\right] \tag{37}$$

The solution is given as

$$\left(\mathbf{v}^{mm}_i\right)^H = \left(\mathbb{E}\left[\dot{\mathbf{y}}^m_{[k],i}\left(\dot{\mathbf{y}}^m_{[k],i}\right)^H\right]\right)^{-1}\left(\mathbb{E}\left[\dot{\mathbf{y}}^m_{[k],i}\left(X^m_{(k),i}\right)^*\right]\right) \tag{38}$$

where $\dot{\mathbf{y}}^m_{[k],i} = \underline{\mathrm{F}}_i \mathbf{y}^m_{[k]}$. The solution can be further written as a function of the channel matrices, input correlation and noise

correlation matrices. The first part of (38) ($\mathbb{E}[\dot{\mathbf{y}}^m_{[k],i}(\dot{\mathbf{y}}^m_{[k],i})^H]$) can be expanded as

$$\mathbb{E}\left[\dot{\mathbf{y}}^m_{[k],i}\left(\dot{\mathbf{y}}^m_{[k],i}\right)^H\right] = \underline{\mathrm{F}}_i\mathbb{E}\left[\mathbf{y}^m_{[k]}\mathbf{y}^{m^H}_{[k]}\right]\underline{\mathrm{F}}_i^H = \underline{\mathrm{F}}_i\mathbf{R}_{\mathbf{y}^m\mathbf{y}^m}\underline{\mathrm{F}}_i^H \tag{39}$$

The second part of (38) ($\mathbb{E}[\dot{\mathbf{y}}^m_{[k],i}(X^m_{(k),i})^*]$) can be expanded as

$$\mathbb{E}\left[\dot{\mathbf{y}}^m_{[k],i}\left(X^m_{(k),i}\right)^*\right] = \mathbb{E}\left[\left(\underline{\mathrm{F}}_i\mathbf{y}^m_{[k]}\right)\left(X^m_{(k),i}\right)^*\right] = \mathbb{E}\left[\left(\underline{\mathrm{F}}_i\sum_{l=1}^{M}\mathbf{H}^{ml}\check{\mathbf{x}}^l_{[k]} + \mathbf{n}^m_{[k]}\right)\left(\check{\mathbf{x}}^m_{[k]}\right)^H\mathbf{e}_i\right] \tag{40}$$

which can be written as a function of known input correlation matrix

$$\mathbb{E}\left[\dot{\mathbf{y}}^m_i[k]\left(X^m_{(k),i}\right)^*\right] = \underline{\mathrm{F}}_i\mathbf{H}^{mm}\mathbf{R}_{\check{\mathbf{x}}^m}\mathbf{e}_i \tag{41}$$

Thus, the optimal solution for the diagonal PTEQ coefficients for user m on tone i is given as (42), at the bottom of the page.

It can be observed that the full MIMO PTEQ and the sparse MIMO PTEQ require signal coordination among users at the receiver side. Hence, the users are required to have their receivers physically co-located. The requirement of signal coordination can be observed from the formulation of the estimated k^{th} transmitted symbol for user m on tone i for both the full MIMO PTEQ and the sparse MIMO PTEQ in (13) and (22), respectively. The required signal coordination at the receiver side is only possible in the upstream scenario where the receivers are co-located at the DPU. In the downstream scenario, since the users are not co-located, the signal coordination at the receiver side is not realizable. Therefore, the full MIMO PTEQ and sparse MIMO PTEQ can not be applied. However, the diagonal MIMO PTEQ does not require signal coordination, as can be observed from the formulation of the estimated k^{th} transmitted symbol for user m on tone i with diagonal PTEQ in (36). Therefore, the diagonal MIMO PTEQ can be applied in both upstream and downstream scenarios.

V. INITIALIZATION COMPUTATIONAL COMPLEXITY

Computing the optimal sparse or diagonal MIMO PTEQ coefficients, can be based on (31) and (42), shown at the bottom of the page if first all the channel matrices (and noise correlation matrices) are estimated. Alternatively these coefficients can be computed based on received data correlations, i.e., with (25) and (38) (and (18) for full MIMO PTEQ). The latter option will be analysed here. Computing the coefficients can then be divided in 3 tasks: (*i*) computing the SDFT of the received signals using the difference terms implementation, (*ii*) computing the correlation matrices of the input signals to the PTEQ and subsequently (*iii*) solving the sets of linear equations to compute the optimal MIMO PTEQ coefficients.

(i) Computing the SDFT of the received signals using the difference terms implementation, as described in (12), requires M DFT operations and $M(T-1)$ complex add operations per DMT symbol. This task is common to all three discussed MIMO PTEQs.

The computational complexity of the remaining tasks is described below.

A. FULL MIMO PTEQ

(ii) Computing the correlation matrix $\mathbb{E}[\ddot{\mathbf{y}}_{[k],i}(\ddot{\mathbf{y}}_{[k],i})^H]$ requires $\mathcal{O}(M^2T^2)$ arithmetic operations, where MT is the length of the vector $\ddot{\mathbf{y}}_{[k],i}$. For $i = 1\cdots N$, the total required number of arithmetic operations becomes $\mathcal{O}(NM^2T^2)$.

(iii) Solving (18) as $(\tilde{\mathbf{v}}^m_i)^H = (\mathbb{E}[\ddot{\mathbf{y}}_{[k],i}(\ddot{\mathbf{y}}_{[k],i})^H])^{-1}\cdot(\mathbb{E}[\ddot{\mathbf{y}}_{[k],i}(X^m_{(k),i})^*])$ can be done with $\mathcal{O}(\frac{1}{3}M^3T^3)$ arithmetic operations. For $i = 1\cdots N$, the total required number of arithmetic operations becomes $\mathcal{O}(\frac{1}{3}NM^3T^3)$.

B. SPARSE MIMO PTEQ

(ii) Computing the correlation matrix $\mathbb{E}[\mathring{\mathbf{y}}^m_{[k],i}(\mathring{\mathbf{y}}^m_{[k],i})^H]$ requires $\mathcal{O}((T+M-1)^2)$ arithmetic operations, where $M+T-1$ is the length of the vector $\ddot{\mathbf{y}}^m_{[k],i}$. For $i = 1\cdots N$ and $m = 1\cdots M$, the total required arithmetic operations becomes $\mathcal{O}(NM(T+M-1)^2)$.

(iii) Solving (25) as $(\tilde{\mathbf{v}}^m_i)^H = (\mathbb{E}[\mathring{\mathbf{y}}^m_{[k],i}(\mathring{\mathbf{y}}^m_{[k],i})^H])^{-1}\cdot(\mathbb{E}[\mathring{\mathbf{y}}^m_{[k],i}(X^m_{(k),i})^*])$ can be done with $\mathcal{O}(\frac{1}{3}(T+M-1)^3)$ arithmetic operations. For $i = 1\cdots N$ and $m = 1\cdots M$, the total required number of arithmetic operations becomes $\mathcal{O}(\frac{1}{3}NM(T+M-1)^3)$.

C. DIAGONAL MIMO PTEQ

(ii) Computing the correlation matrix $\mathbb{E}[\dot{\mathbf{y}}^m_{[k],i}(\dot{\mathbf{y}}^m_{[k],i})^H]$ requires $\mathcal{O}(T^2)$ arithmetic operations, where T is

$$\left(\tilde{\mathbf{v}}^m_i\right)^H = \left(\underline{\mathrm{F}}^m_i\begin{bmatrix}\sum_{l=1}^{M}\mathbf{H}^{1,l}\mathbf{R}_{\check{\mathbf{x}}^l}\mathbf{H}^{1,l^H}+\mathbf{R}_{\mathbf{n}^1} & \sum_{l=1}^{M}\mathbf{H}^{1,l}\mathbf{R}_{\check{\mathbf{x}}^l}\mathbf{H}^{2,l^H} & \cdots & \sum_{l=1}^{M}\mathbf{H}^{1,l}\mathbf{R}_{\check{\mathbf{x}}^l}\mathbf{H}^{M,l^H}\\ \sum_{l=1}^{M}\mathbf{H}^{2,l}\mathbf{R}_{\check{\mathbf{x}}^l}\mathbf{H}^{1,l^H} & \sum_{l=1}^{M}\mathbf{H}^{2,l}\mathbf{R}_{\check{\mathbf{x}}^l}\mathbf{H}^{2,l^H}+\mathbf{R}_{\mathbf{n}^2} & \cdots & \sum_{l=1}^{M}\mathbf{H}^{2,l}\mathbf{R}_{\check{\mathbf{x}}^l}\mathbf{H}^{M,l^H}\\ \vdots & \vdots & \ddots & \vdots\\ \sum_{l=1}^{M}\mathbf{H}^{M,l}\mathbf{R}_{\check{\mathbf{x}}^l}\mathbf{H}^{1,l^H} & \sum_{l=1}^{M}\mathbf{H}^{M,l}\mathbf{R}_{\check{\mathbf{x}}^l}\mathbf{H}^{2,l^H} & \cdots & \sum_{l=1}^{M}\mathbf{H}^{M,l}\mathbf{R}_{\check{\mathbf{x}}^l}\mathbf{H}^{M,l^H}+\mathbf{R}_{\mathbf{n}^M}\end{bmatrix}\underline{\mathrm{F}}^{m^H}_i\right)^{-1}\underline{\mathrm{F}}^m_i\begin{bmatrix}\mathbf{H}^{1m}\mathbf{R}_{\check{\mathbf{x}}^m}\mathbf{e}_i\\ \mathbf{H}^{2m}\mathbf{R}_{\check{\mathbf{x}}^m}\mathbf{e}_i\\ \vdots\\ \mathbf{H}^{Mm}\mathbf{R}_{\check{\mathbf{x}}^m}\mathbf{e}_i\end{bmatrix} \tag{31}$$

$$\left(\mathbf{v}^{mm}_i\right)^H = \left(\underline{\mathrm{F}}_i\left(\sum_{l=1}^{M}\mathbf{H}^{m,l}\mathbf{R}_{\check{\mathbf{x}}^l}\mathbf{H}^{m,l^H}+\mathbf{R}_{\mathbf{n}^m}\right)\underline{\mathrm{F}}_i^H\right)^{-1}\underline{\mathrm{F}}_i\,\mathbf{H}^{mm}\,\mathbf{R}_{\check{\mathbf{x}}^m}\,\mathbf{e}_i \tag{42}$$

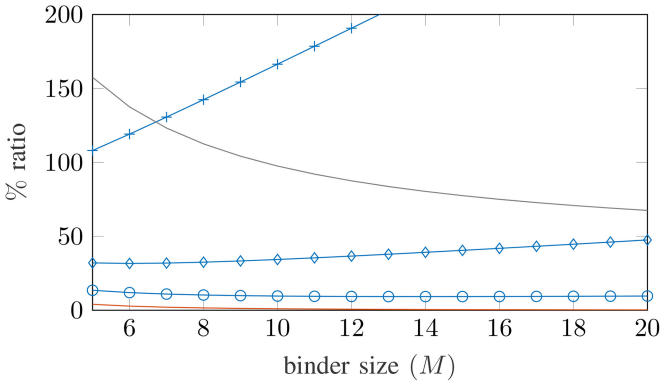

FIGURE 5. % ratio of initialization computational complexity of sparse MIMO PTEQ with PTEQ order-1 (—+—), order-3 (—◇—), order-7 (—○—), diagonal MIMO PTEQ (——) and MIMO TEQ order-7 (——) compared to a full MIMO PTEQ with the same filter order.

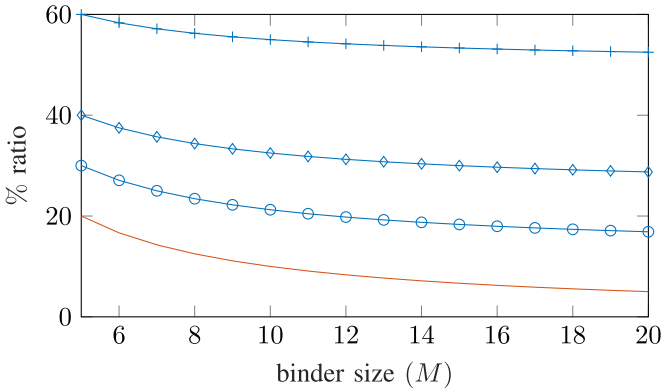

FIGURE 6. % ratio in memory requirement (and runtime computational complexity) of sparse MIMO PTEQ with PTEQ order-1 (—+—), order-3 (—◇—), order-7 (—○—) and diagonal MIMO PTEQ (——) compared to a full MIMO PTEQ with the same filter order.

the length of the vector $\dot{\mathbf{y}}^m_{[k],i}$. For $i = 1 \cdots N$ and $m = 1 \cdots M$, the total required number of arithmetic operations becomes $\mathcal{O}(NMT^2)$.

(iii) Solving (38) as $(\mathbf{v}_i^{mm})^H = (\mathbb{E}[\dot{\mathbf{y}}^m_{[k],i}(\dot{\mathbf{y}}^m_{[k],i})^H])^{-1} \cdot (\mathbb{E}[\dot{\mathbf{y}}^m_{[k],i}(X^m_{(k),i})^*])$ can be done with $\mathcal{O}(\frac{1}{3}T^3)$ arithmetic operations. For $i = 1 \cdots N$ and $m = 1 \cdots M$, the total required number of arithmetic operations becomes $\mathcal{O}(\frac{1}{3}NMT^3)$.

Fig. 5 shows the % ratio of the initialization computational complexity of a sparse MIMO PTEQ and a diagonal MIMO PTEQ compared to a full MIMO PTEQ, for different MIMO PTEQ orders. The % ratio is calculated based on the computationally most expensive task in computing the optimal MIMO PTEQ coefficients, which corresponds to solving (18), (25) and (38) for the full, sparse and diagonal MIMO PTEQ, respectively. The % ratio is calculated as:

$$\%\text{ratio} = \frac{\text{complexity (sparse or diagonal MIMO PTEQ)}}{\text{complexity (full MIMO PTEQ)}} \times 100. \tag{43}$$

Fig. 5 also includes the % ratio of the initialization computational complexity of a UNCDc-Zxc design method based MIMO TEQ (order 7) [9] compared to a full MIMO PTEQ (order 7). The lower orders of MIMO TEQ shows much higher % ratio of the initialization computational complexity compared to a full MIMO PTEQ of the same order and hence are omitted from Fig. 5. Furthermore, since, the computationally most expensive task in computing the optimal MIMO PTEQ coefficients for both the diagonal MIMO PTEQ and full MIMO PTEQ depends on T^3, it can be observed that the % ratio of the initialization computational complexity for the diagonal MIMO PTEQ is independent of the equalizer order. Finally, it can be noticed that the sparse MIMO PTEQ provides a reduction in the initialization computational complexity compared to a full MIMO PTEQ for all filter orders larger than 1. For filter order 1, it can be observed from (43) that the sparse MIMO PTEQ has a higher initialization computational complexity compared to a full MIMO PTEQ. This is because, for the sparse MIMO PTEQ, the filter coefficients are computed separately for each user m (25). However, for the full MIMO PTEQ the filter coefficients for all the users are computed jointly (18). Therefore in the sparse MIMO PTEQ, for lower filter orders, the increase in the computational cost caused by the separate computations of filter coefficients for each user becomes more prominent than the decrease in the computational cost caused by the reduction in the required filter coefficients to be computed, compared to a full MIMO PTEQ.

VI. MEMORY REQUIREMENT

In comparison to a MIMO TEQ, a full MIMO PTEQ needs to store N times more filter coefficients, which hinders its applicability in practical scenarios. Compared to a full MIMO PTEQ, the proposed sparse MIMO PTEQ and the diagonal MIMO PTEQ show a significant reduction in the memory requirement to store the PTEQ coefficients ($\mathbf{V}_i$). A full MIMO PTEQ as shown in (15), requires NM^2T coefficients to be stored. A sparse MIMO PTEQ, as shown in (21), requires $NM(M + T - 1)$ coefficients to be stored. A diagonal MIMO PTEQ, as shown in (34) requires only NMT coefficients to be stored. An equivalent reduction can be seen in the runtime computational complexity. A full MIMO PTEQ performs NM^2T complex multiplications to compute the filtered outputs, while a sparse and a diagonal MIMO PTEQ perform $NM(M + T - 1)$ and NMT complex multiplications respectively to compute the filtered outputs. Fig. 6 shows the % ratio of memory requirement and the runtime computational complexity for a sparse MIMO PTEQ and a diagonal MIMO PTEQ compared to a full MIMO PTEQ, for different MIMO PTEQ orders. The % ratio in Fig. 6 is based on (43) for memory requirement and runtime complexity. Similar to the initialization computational complexity ratio in Fig. 5, it can be noted that the % ratio in the memory requirement and the runtime computational complexity for the diagonal MIMO PTEQ is also independent of the equalizer order, as the memory requirement and

TABLE 1. Simulation parameters.

Parameter	Value
G.fast Profile	106b
Maximum aggregated transmit power (P_g)	8 dBm
Subcarrier spacing	51.75 kHz
DFT size (N)	4096
SNR gap (Γ)	10 dB
Bandwidth	106 MHz
Noise PSD	-140 dBm/Hz

the runtime computational complexity for both the diagonal MIMO PTEQ and full MIMO PTEQ depends on T.

VII. RESULTS

The simulation setup is kept similar to [9]. The G.fast 106b profile [28] is considered here for the simulation of a 5×5 MIMO DSL system, i.e., a 5-line DSL system with 2048 tones. A total transmit power of 8 dBm and a noise power of -140 dBm/Hz is considered. A practical approach is chosen for the transmit power distribution over tones as follows. Initially, the power is allocated to tones according to the power spectral density (PSD) mask specification [29]. Based on that, a PTEQ filter is designed and the number of bits that can be transmitted on each tone is calculated. The tones for which the number of transmitted bits is smaller than 1, are rejected and left unused. The remaining power is finally distributed over the used tones,while making sure not to violate the PSD mask constraints [29], and then the PTEQ filter coefficients are updated one last time. The simulations are performed for both a theoretical channel model and measured channels. The theoretical channel (length 600m) is based on the KHM model, suggested in [30], while the measured channel data corresponds to cable binders of two Tier-1 operators (channel 1 of length 728m and channel 2 of length 600m). The data rates are computed with a bit-cap of 14 bits. Moreover for the simulations, the input correlation matrices ($\mathbf{R}_{\ddot{\mathbf{x}}^j}$) are considered to be diagonal, assuming that the transmitted symbols $\ddot{\mathbf{x}}^j_{(k)}$ are proper,—i.e., that their real and imaginary parts are uncorrelated and have equal variance—and are independent over users, tones, and time. Furthermore, we assume perfect knowledge of the channel state information (CSI). This assumption is standard in wireline communication systems, especially in DSL systems [31]. Table 1 summarizes the simulation parameters.

Fig. 7(a), Fig. 7(b) and Fig. 7(c) compare the performance of the full MIMO PTEQ with the proposed sparse MIMO PTEQ in terms of total achieved rates for a five line DSL system, for different channels. The rates are calculated over a range of synchronisation delays, to also characterize the robustness of the MIMO PTEQ design against the synchronization delay. From the simulation results, it can be noticed that the sparse PTEQ attains similar performance as the full MIMO PTEQ, while providing a reduction in the initialization computational complexity and the memory requirement. As discussed in Section III, the ISI and ICI power caused by crosstalk channels is expected to be small. Hence, ignoring the crosstalk ISI and ICI cancellation indeed does not significantly affect the performance of the MIMO PTEQ and a single tap equalizer for crosstalk cancellation works similar to a T tap equalizer. Furthermore, it can be observed from Fig. 7(a), Fig. 7(b) and Fig. 7(c) that the performance of the full MIMO PTEQ and sparse MIMO PTEQ shows insignificant improvement, while increasing the order from PTEQ order 1 to PTEQ order 7. This suggests that the channel impulse responses used for the simulations can be approximated with a rational transfer function that has few poles and an order-1 MIMO PTEQ is already good enough to cancel them. An impulse response whose approximated rational transfer function has a higher number of poles will require a higher order PTEQ, and the system performance will not saturate at order-1 MIMO PTEQ.

Fig. 7(d), Fig. 7(e) and Fig. 7(f) compare the performance of the full MIMO PTEQ and the proposed diagonal MIMO PTEQ. Though the diagonal PTEQ further reduces the initialization computational complexity and memory requirement, an average performance drop of 29.3% is observed in the absence of crosstalk cancellation. This drop in performance can likely be avoided by using crosstalk precompensation, also referred to as downstream vectoring, at the transmitter side, but designing the vectoring together with the diagonal MIMO PTEQ is complex and remains as a topic for future work.

Fig. 8 extends the results of Fig. 7 with the same channels and simulation parameters but with a CP length of 64 samples. Finally, Fig. 9 provides simulation results for non-LR-G.fast channels. The theoretical channel (length 300m) is again based on the KHM model, suggested in [30], while the measured channel data corresponds to cable binders of two Tier-1 operators (channel 1 of length 250m and channel 2 of length 300m). The simulation parameters are kept the same (Table 1) with a CP length of 64 samples. The results in Fig. 8 and Fig. 9 further bolster the conclusions drawn from Fig. 7.

VIII. CONCLUSION

The paper is motivated by the potential use of a MIMO PTEQ in newly emerging LR-xDSL and tackles the large initialization computational complexity and memory requirement for the full MIMO PTEQ. A specific structure in the MIMO DSL channel is exploited, namely that the combined ISI and ICI signal power from the crosstalk channels is significantly lower than the desired and combined ISI and ICI signal power from the direct channels, to derive a very low complexity/memory solution, referred as sparse MIMO PTEQ, with negligible impact ($\approx 0.5\%$ drop) on the performance compared to a full MIMO PTEQ. For a conventional DSL binder size of 16 lines and a PTEQ order of 3, the proposed sparse MIMO PTEQ operates at 42% of the initialization computational complexity and 29.7% of the memory requirement, with negligible performance degradation, compared to a full MIMO PTEQ. Even larger reductions in initialization computational complexity and memory requirement are achieved by the proposed diagonal MIMO PTEQ, which operates at 0.4% of the initialization computational

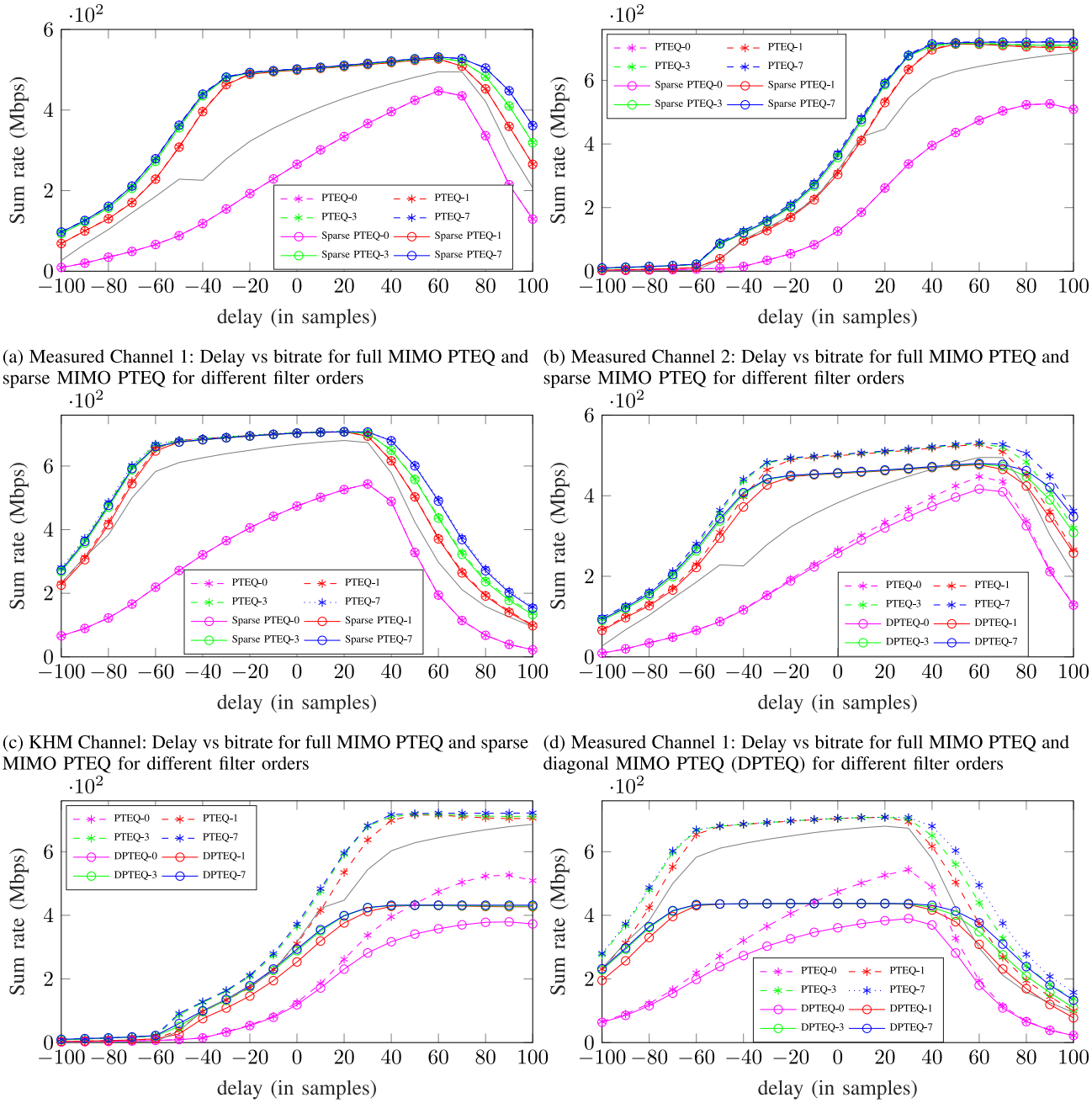

(a) Measured Channel 1: Delay vs bitrate for full MIMO PTEQ and sparse MIMO PTEQ for different filter orders

(b) Measured Channel 2: Delay vs bitrate for full MIMO PTEQ and sparse MIMO PTEQ for different filter orders

(c) KHM Channel: Delay vs bitrate for full MIMO PTEQ and sparse MIMO PTEQ for different filter orders

(d) Measured Channel 1: Delay vs bitrate for full MIMO PTEQ and diagonal MIMO PTEQ (DPTEQ) for different filter orders

(e) Measured Channel 2: Delay vs bitrate for full MIMO PTEQ and diagonal MIMO PTEQ (DPTEQ) for different filter orders

(f) KHM Channel: Delay vs bitrate for full MIMO PTEQ and diagonal MIMO PTEQ (DPTEQ) for different filter orders

FIGURE 7. Performance comparison of MIMO PTEQ structures (and MIMO TEQ-3 (_____) [9]) for different DSL channels and filter orders (CP = 128).

complexity and 6.25% of the memory requirement compared to a full MIMO PTEQ. It also allows the MIMO PTEQ implementation in upstream as well as downstream scenarios. However, in absence of crosstalk cancellation the performance of diagonal MIMO PTEQ drops significantly compared to a full MIMO PTEQ. This drop in performance can likely be avoided by using crosstalk precompensation (i.e., downstream vectoring) at the transmitter side. Finally, the applicability of the proposed models could potentially be interesting for wireless systems as well, which are characterized by a similar structure.

APPENDIX
OPTIMAL MIMO PTEQ COEFFICIENTS

The optimization problem (MMSE) for optimal PTEQ filter coefficients for user m and tone i is given as

$$\underset{\tilde{\mathbf{v}}_i^m}{\text{minimize}} \quad \mathbb{E}\left[\left|\tilde{\mathbf{v}}_i^m \ddot{\mathbf{y}}_{[k],i} - X_{(k),i}^m\right|^2\right] \tag{44}$$

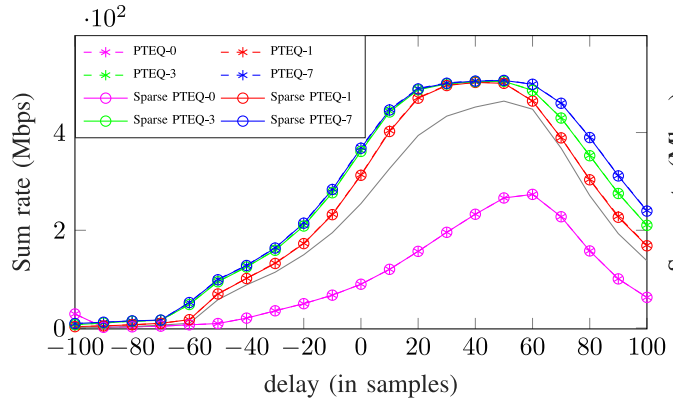

(a) Measured Channel 1: Delay vs bitrate for full MIMO PTEQ and sparse MIMO PTEQ for different filter orders

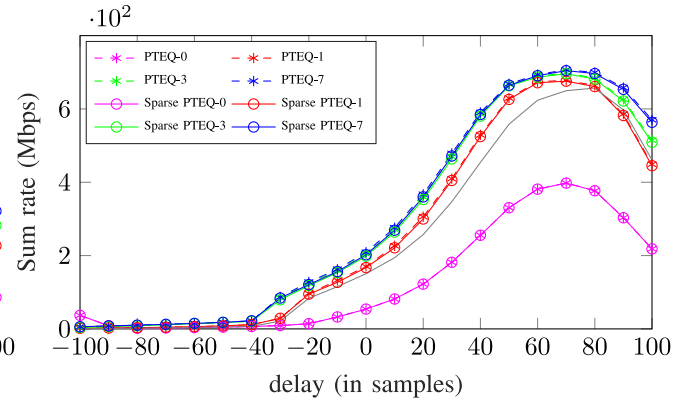

(b) Measured Channel 2: Delay vs bitrate for full MIMO PTEQ and sparse MIMO PTEQ for different filter orders

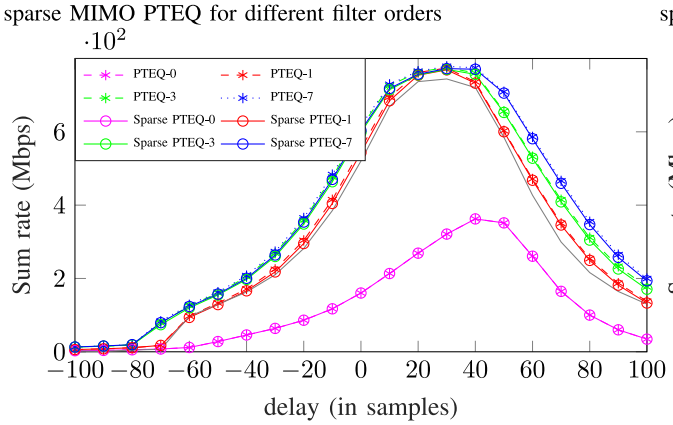

(c) KHM Channel: Delay vs bitrate for full MIMO PTEQ and sparse MIMO PTEQ for different filter orders

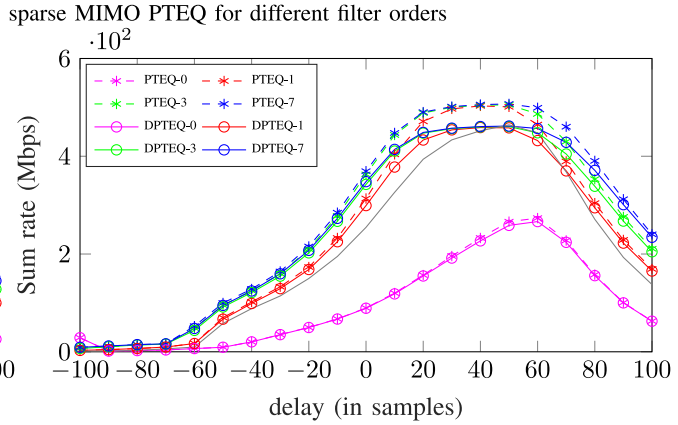

(d) Measured Channel 1: Delay vs bitrate for full MIMO PTEQ and diagonal MIMO PTEQ (DPTEQ) for different filter orders

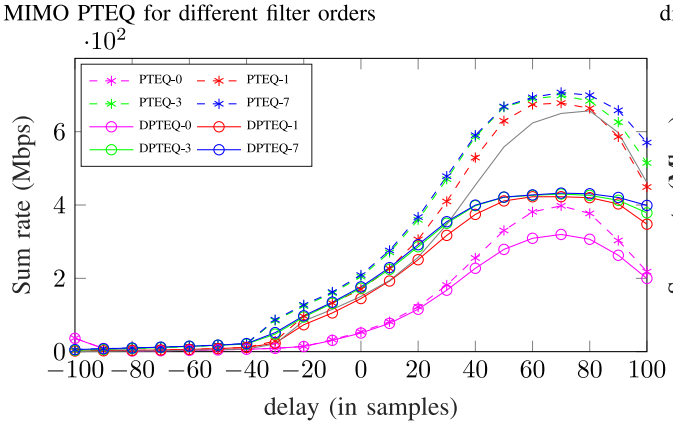

(e) Measured Channel 2: Delay vs bitrate for full MIMO PTEQ and diagonal MIMO PTEQ (DPTEQ) for different filter orders

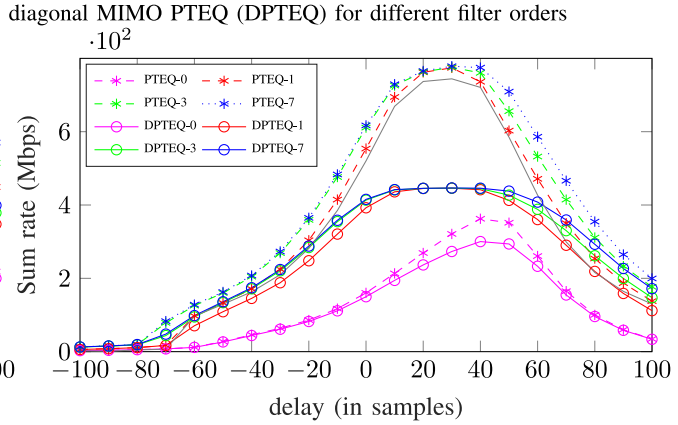

(f) KHM Channel: Delay vs bitrate for full MIMO PTEQ and diagonal MIMO PTEQ (DPTEQ) for different filter orders

FIGURE 8. **Performance comparison of MIMO PTEQ structures (and MIMO TEQ-3 (_____) [9]) for different DSL channels and filter orders (CP = 64).**

where $\ddot{\mathbf{y}}_{[k],i} = \underline{\check{F}}_i \cdot \check{\mathbf{y}}_{[k]}$. The mean squared error can be expanded as

$$\begin{aligned}\varepsilon_i^m &= \mathbb{E}\left[\left(\tilde{\mathbf{v}}_i^m\ddot{\mathbf{y}}_{[k],i} - X_{(k),i}^m\right)\left(\tilde{\mathbf{v}}_i^m\ddot{\mathbf{y}}_{[k],i} - X_{(k),i}^m\right)^H\right] \\ &= \tilde{\mathbf{v}}_i^m\mathbb{E}\left[\ddot{\mathbf{y}}_{[k],i}\left(\ddot{\mathbf{y}}_{[k],i}\right)^H\right]\left(\tilde{\mathbf{v}}_i^m\right)^H - \tilde{\mathbf{v}}_i^m\mathbb{E}\left[\ddot{\mathbf{y}}_{[k],i}\left(X_{(k),i}^m\right)^H\right] \\ &\quad - \mathbb{E}\left[X_{(k),i}^m\left(\ddot{\mathbf{y}}_{[k],i}\right)^H\right]\left(\tilde{\mathbf{v}}_i^m\right)^H + \mathbb{E}\left[X_{(k),i}^m\left(X_{(k),i}^m\right)^H\right] \quad (45)\end{aligned}$$

Taking the derivative of the mean squared error with respect to $(\tilde{\mathbf{v}}_i^m)^H$ yields

$$\frac{\partial\varepsilon_i^m}{\partial\left(\tilde{\mathbf{v}}_i^m\right)^H} = 2\mathbb{E}\left[\ddot{\mathbf{y}}_{[k],i}\left(\ddot{\mathbf{y}}_{[k],i}\right)^H\right]\left(\tilde{\mathbf{v}}_i^m\right)^H - 2\mathbb{E}\left[\ddot{\mathbf{y}}_{[k],i}\left(X_{(k),i}^m\right)^H\right] \quad (46)$$

Equating the derivative to 0 to find the optimal $\tilde{\mathbf{v}}_i^m$ yields

$$\left(\tilde{\mathbf{v}}_i^m\right)^H = \mathbb{E}\left[\ddot{\mathbf{y}}_{[k],i}\left(\ddot{\mathbf{y}}_{[k],i}\right)^H\right]^{-1}\mathbb{E}\left[\ddot{\mathbf{y}}_{[k],i}\left(X_{(k),i}^m\right)^*\right]. \quad (47)$$

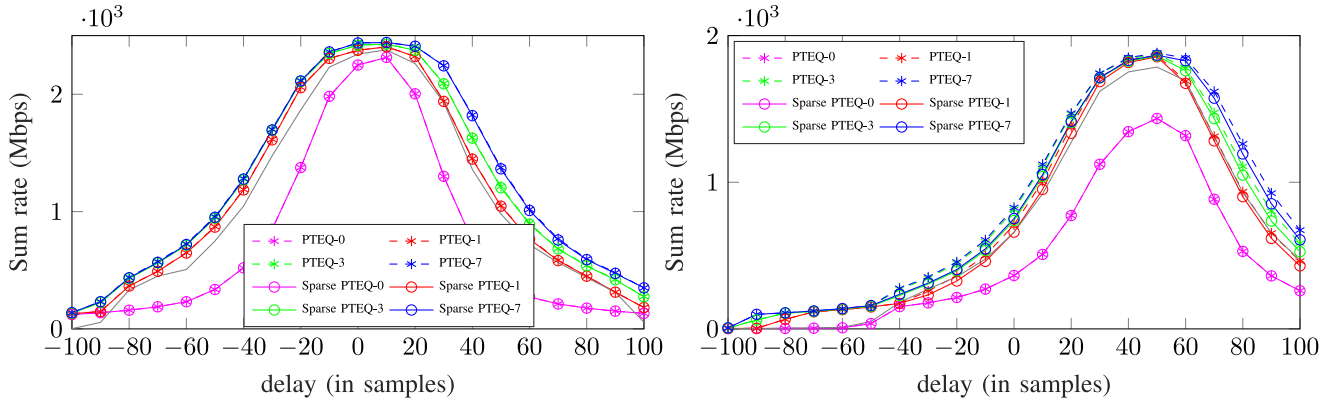

(a) Measured Channel 1: Delay vs bitrate for full MIMO PTEQ and sparse MIMO PTEQ for different filter orders

(b) Measured Channel 2: Delay vs bitrate for full MIMO PTEQ and sparse MIMO PTEQ for different filter orders

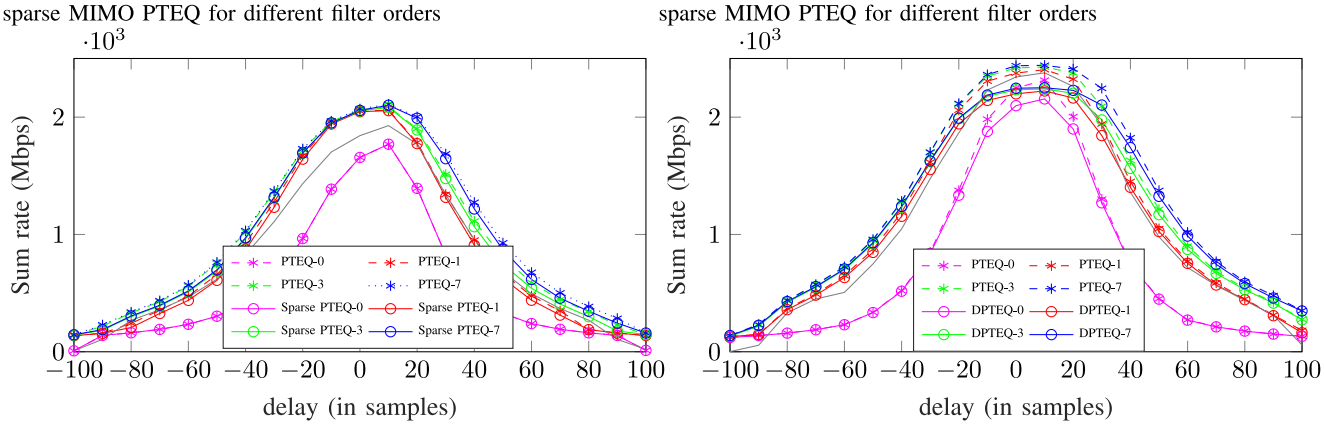

(c) KHM Channel: Delay vs bitrate for full MIMO PTEQ and sparse MIMO PTEQ for different filter orders

(d) Measured Channel 1: Delay vs bitrate for full MIMO PTEQ and diagonal MIMO PTEQ (DPTEQ) for different filter orders

(e) Measured Channel 2: Delay vs bitrate for full MIMO PTEQ and diagonal MIMO PTEQ (DPTEQ) for different filter orders

(f) KHM Channel: Delay vs bitrate for full MIMO PTEQ and diagonal MIMO PTEQ (DPTEQ) for different filter orders

FIGURE 9. **Performance comparison of MIMO PTEQ structures (and MIMO TEQ-3 (_____) [9]) for different DSL channels (non-LR-G.fast) and filter orders (CP = 64).**

REFERENCES

[1] "Europe's Digital Progress Report 2017." European Commission. Aug. 2017. [Online]. Available: https://ec.europa.eu/digital-single-market/en/news/europes-digital-progress-report-2017

[2] M. Timmers, K. Hooghe, M. Guenach, and J. Maes, "Digital complexity in DSL: An extrapolated historical overview," in *Proc. 2nd Int. Conf. Access Netw.*, May 2011, pp. 19–23. [Online]. Available: http://www.thinkmind.org/index.php?view=article&articleid=access_2011_2_10_40045

[3] "Asymmetric digital subscriber line (ADSL) transceivers," Int. Telecommun. Union, Geneva, Switzerland, ITU-Recommendation G. 992.1, 1999.

[4] N. Al-Dhahir and J. M. Cioffi, "Optimum finite-length equalization for multicarrier transceivers," *IEEE Trans. Commun.*, vol. 44, no. 1, pp. 56–64, Jan. 1996.

[5] "Very high speed digital subscriber line transceivers 2 (VDSL2) recommendation," Int. Telecommun. Union, Geneva, Switzerland, ITU-Recommendation G.993.2, 2019.

[6] V. Oksman *et al.*, "The ITU-T's new G.fast standard brings DSL into the gigabit era," *IEEE Commun. Mag.*, vol. 54, no. 3, pp. 118–126, Mar. 2016.

[7] V. Oksman *et al.*, "MGFAST: A new generation of copper broadband access," *IEEE Commun. Mag.*, vol. 57, no. 8, pp. 14–21, Aug. 2019.

[8] *Long Reach VDSL (LR-VDSL) Trial: Service and Interface Description*, document STIN 522, Brit. Telecommun., London, U.K., Aug. 2016. [Online]. Available: https://docplayer.net/35907784-Stin-522-issue-1-august-2016.html
[9] M. Sharma, M. Moonen, Y. Lefevre, and P. Tsiaflakis, "MIMO time domain equalizer design for long reach xDSL MIMO channel shortening," *IEEE Access*, vol. 8, pp. 203468–203477, 2020.
[10] K. VanAcker, "Equalization and echo cancellation for DMT-based DSL modems," Ph.D. dissertation, Dept. Elektrotechniek, Katholieke Universiteit Leuven, Leuven, Belgium, 2001.
[11] G. Ysebaert, F. Pisoni, M. Bonaventura, R. Hug, and M. Moonen, "Echo cancellation in DMT-receivers: Circulant decomposition canceler," *IEEE Trans. Signal Process.*, vol. 52, no. 9, pp. 2612–2624, Sep. 2004.
[12] F. Lindqvist and A. Fertner, "Frequency domain echo canceller for DMT-based systems," *IEEE Signal Process. Lett.*, vol. 18, no. 12, pp. 713–716, Dec. 2011.
[13] K. Vanbleu, G. Ysebaert, G. Cuypers, M. Moonen, and K. Van Acker, "Bitrate-maximizing time-domain equalizer design for DMT-based systems," *IEEE Trans. Commun.*, vol. 52, no. 6, pp. 871–876, Jun. 2004.
[14] G. Altin and R. K. Martin, "Bit-error-rate-minimizing channel shortening using post-feq diversity combining and a genetic algorithm," *Signal Process.*, vol. 91, no. 4, pp. 1021–1031, 2011. [Online]. Available: https://www.sciencedirect.com/science/article/pii/S0165168410003798
[15] C. Toker and G. Altin, "Blind, adaptive channel shortening equalizer algorithm which can provide shortened channel state information (BACS-SI)," *IEEE Trans. Signal Process.*, vol. 57, no. 4, pp. 1483–1493, Apr. 2009.
[16] K. Vanbleu, G. Ysebaert, G. Cuypers, and M. Moonen, "On the relation between time-domain equalizers and per-tone equalizers for DMT-based systems," in *Proc. IEEE Benelux Signal Process. Symp.*, 2004, pp. 16–17.
[17] K. VanAcker, G. Leus, M. Moonen, O. van de Wiel, and T. Pollet, "Per tone equalization for DMT-based systems," *IEEE Trans. Commun.*, vol. 49, no. 1, pp. 109–119, Jan. 2001.
[18] G. Leus and M. Moonen, "Per-tone equalization for MIMO OFDM systems," *IEEE Trans. Signal Process.*, vol. 51, no. 11, pp. 2965–2975, Nov. 2003.
[19] J. Verdyck, Y. Lefevre, P. Tsiaflakis, and M. Moonen, "Per-tone precoding and per-tone equalization for OFDM and DMT transmission systems: Duality, filter optimization, and resource allocation," *IEEE Open J. Signal Process.*, vol. 1, pp. 257–273, 2020.
[20] M. Guenach, J. Meas, M. Timmers, O. Lamparter, J.-C. Bischoff, and M. Peeters, "Vectoring in DSL systems: Practices and challenges," in *Proc. IEEE Global Telecommun. Conf.*, 2011, pp. 1–6.
[21] P. K. Pandey, M. Moonen, and L. Deneire, "MMSE-based partial crosstalk cancellation for upstream VDSL," *Signal Process.*, vol. 92, no. 7, pp. 1602–1610, 2012. [Online]. Available: https://www.sciencedirect.com/science/article/pii/S0165168411004476
[22] R. Cendrillon, G. Ginis, E. Van Den Bogaert, and M. Moonen, "A near-optimal linear crosstalk canceler for upstream VDSL," *IEEE Trans. Signal Process.*, vol. 54, no. 8, pp. 3136–3146, Aug. 2006.
[23] F. Sjoberg, R. Nilsson, M. Isaksson, P. Odling, and P. O. Borjesson, "Asynchronous zipper [subscriber line duplex method]," in *Proc. IEEE Int. Conf. Commun.*, vol. 1, 1999, pp. 231–235.
[24] G. Taubock, "Complex noise analysis of DMT," *IEEE Trans. Signal Process.*, vol. 55, no. 12, pp. 5739–5754, Dec. 2007.
[25] R. Strobel, *Channel Modeling and Physical Layer Optimization in Copper Line Networks* (Signals and Communication Technology). Cham, Switzerland: Springer, 2019.
[26] J. Verdyck, Y. Lefevre, P. Tsiaflakis, and M. Moonen, "Signal impropriety in discrete multi-tone systems and widely linear per-tone equalization," *IEEE Open J. Commun. Soc.*, vol. 2, pp. 367–383, 2021.
[27] W. A. Martins, F. Cruz-Roldán, M. Moonen, and P. S. R. Diniz, "Intersymbol and intercarrier interference in OFDM transmissions through highly dispersive channels," in *Proc. 27th Eur. Signal Process. Conf. (EUSIPCO)*, 2019, pp. 1–5.
[28] "Fast access to subscriber terminals (G.fast)—Physical layer specification," ITU-T Study Group 15, Int. Telecommun. Union, Geneva, Switzerland, Rep. ITU-T G.9701, 2015.
[29] "Fast access to subscriber terminals (G.fast)—Power spectral density specification," ITU-T Study Group 15, Int. Telecommun. Union, Geneva, Switzerland, Rep. ITU-T G.9700, 2014.
[30] D. Acatauassu, S. Höst, C. Lu, M. Berg, A. Klautau, and P. O. Börjesson, "Simple and causal copper cable model suitable for G.fast frequencies," *IEEE Trans. Commun.*, vol. 62, no. 11, pp. 4040–4051, Nov. 2014.
[31] S. M. Zafaruddin, I. Bergel, and A. Leshem, "Signal processing for gigabit-rate wireline communications: An overview of the state of the art and research challenges," *IEEE Signal Process. Mag.*, vol. 34, no. 5, pp. 141–164, Sep. 2017.

MOHIT SHARMA received the M.Sc. degree in communication engineering from RWTH Aachen University, Germany, in 2018. He is currently pursuing the Ph.D. degree in electrical engineering with KU Leuven, Belgium, under the supervision of Prof. M. Moonen. His research interest includes digital signal processing, information theory, and optimization applications with a focus on MIMO communication systems.

JEROEN VERDYCK (Student Member, IEEE) received the M.Sc. and Ph.D. degrees in electrical engineering from KU Leuven, in 2014 and 2021, respectively. He has been involved in joint projects with Nokia Bell Labs, Antwerp, Belgium, and with the University of Antwerp, Antwerp. He joined GN Advanced Science, Eindhoven, The Netherlands, in 2021. As a Research Scientist, he currently works on audio signal processing algorithms for hearing aids. His research interests include signal processing, numerical optimization, and machine learning with applications in digital communication systems and audio signal processing. He received the ICC 2017 TAOS Best Paper Award (with Jeremy Van den Eynde).

YANNICK LEFEVRE received the master's degree in engineering sciences from Vrije Universiteit Brussel (VUB), Brussels, Belgium, and Universiteit Gent, Ghent, Belgium, in 2010, and the Ph.D. degree in applied sciences and engineering from VUB, in 2014. He joined Nokia Bell Labs, Antwerp, Belgium, in 2015. As a Research Engineer, he works on next-generation copper and optical access technologies. His research interests include digital signal processing, forward error correction, signal shaping, and modulation. He was a recipient of an Aspirant Grant from the Research Foundation-Flanders.

PASCHALIS TSIAFLAKIS received the M.Sc. and Ph.D. degrees in electrical engineering from KU Leuven, in 2004 and 2009, respectively. He has further conducted research with Princeton University, UCLA, Tsinghua University, and UC Louvain. Since 2013, he has been with Nokia Bell Labs, where his main activities focus on research and innovation, contributing to standardization bodies, and driving innovation into next-generation communication products. He has performed research in fields of optimization, signal processing, and machine learning, with applications to wireline and wireless communication systems. He received both the Ph.D. and Postdoctoral Fellowship of the Research Foundation Flanders, the Belgian Young ICT Personality Award, in 2010, the Nokia Innovation Award, in 2017, the Nokia Bell Top Inventor Award, in 2019, the Distinguished Member of Technical Staff Title, in 2019, and several IEEE Best Paper Awards.

MARC MOONEN (Fellow, IEEE) is a Full Professor with the Electrical Engineering Department, KU Leuven, where he is Heading a Research Team working in the area of numerical algorithms and signal processing for digital communications, wireless communications, DSL, and audio signal processing.

He received the 1994 KU Leuven Research Council Award, the 1997 Alcatel Bell (Belgium) Award (with Piet Vandaele), the 2004 Alcatel Bell (Belgium) Award (with Raphael Cendrillon), and was a 1997 Laureate of the Belgium Royal Academy of Science. He received the journal best paper awards from the IEEE TRANSACTIONS ON SIGNAL PROCESSING (with Geert Leus and with Daniele Giacobello) and from *Signal Processing* (Elsevier) (with Simon Doclo). He was the Chairman of the IEEE Benelux Signal Processing Chapter from 1998 to 2002, a member of the IEEE Signal Processing Society Technical Committee on Signal Processing for Communications, and the President of European Association for Signal Processing, (EURASIP) from 2007 to 2008 and from 2011 to 2012. He has served as the Editor-in-Chief for the *EURASIP Journal on Applied Signal Processing* from 2003 to 2005, an Area Editor for Feature Articles in *IEEE Signal Processing Magazine* from 2012 to 2014, and has been a Member of the Editorial Board of *Signal Processing*, IEEE TRANSACTIONS ON CIRCUITS AND SYSTEMS—PART II: EXPRESS BRIEFS, *IEEE Signal Processing Magazine*, *Integration-the VLSI Journal*, *EURASIP Journal on Wireless Communications and Networking*, and *EURASIP Journal on Advances in Signal Processing*. He is a Fellow of EURASIP in 2018.